

## Research Article

# Couple-Stress Fluid Improves Dynamic Response of Gear-Pair System Supported by Journal Bearings

Cai-Wan Chang-Jian,<sup>1</sup> Shiuh Ming Chang,<sup>2</sup>  
and Hsieh-Chung Hsu<sup>1</sup>

<sup>1</sup> Department of Mechanical and Automation Engineering, I-Shou University, 1, Section 1, Syuecheng Road, Dashu District, Kaohsiung 84001, Taiwan

<sup>2</sup> Department of Mechanical and Automation Engineering, Kao Yuan University, Kaohsiung 82151, Taiwan

Correspondence should be addressed to Cai-Wan Chang-Jian, cwchangjian@mail.isu.edu.tw

Received 6 July 2011; Accepted 18 August 2011

Academic Editor: Nazim I. Mahmudov

Copyright © 2012 Cai-Wan Chang-Jian et al. This is an open access article distributed under the Creative Commons Attribution License, which permits unrestricted use, distribution, and reproduction in any medium, provided the original work is properly cited.

A systematic analysis of the dynamic behavior of a gear-bearing system with nonlinear suspension, couple-stress fluid flow effect, nonlinear oil-film force, and nonlinear gear mesh force is performed in the present study. The dynamic orbits of the system are observed using bifurcation diagrams plotted using the dimensionless rotational speed ratio as a control parameter. The onset of chaotic motion is identified from the phase diagrams, power spectra, Poincaré maps, Lyapunov exponents and fractal dimension of the gear-bearing system. The numerical results reveal that the system exhibits a diverse range of periodic, subharmonic, quasiperiodic, and chaotic behaviors. The couple-stress fluid would be a useful lubricating fluid to suppress nonlinear dynamic responses and improve the steady of the systems. The results presented in this study provide some useful insights into the design and development of a gear-bearing system for rotating machinery that operates in highly rotational speed and highly nonlinear regimes.

## 1. Introduction

Lubricants with additives are often considered as non-Newtonian fluids and are found to be able to be used to improve the properties of lubricants such as the viscosity of lubricants in many studies and also many applications. According to the results of experiments, it is evidenced that the use of small amounts of suitable additives can improve lubricant properties. It can make the viscosity of the lubricant to be independent of the temperature. With the development of modern machine elements, the increasing use of complex fluids as lubricants has been emphasized. Oliver [1] had found that the presence of dissolved polymer in the lubricant could increase the load-carrying capacity and decrease the friction. Spikes [2] showed that the base oil blending with additives could reduce the friction and the surface damage in

elastohydrodynamic contacts. Because of the behavior of the complex fluids violates the linear shear-stress-rate relationship, it fails to describe the rheological behaviour of the non-Newtonian fluid. Therefore, a different microcontinuum theory has been developed to better describe the rheological behaviour of the non-Newtonian fluid. Shehawey and Mekheimer [3] applied the couple-stress model to analyze the peristalsis problem for its relative mathematical simplicity. Das [4] proposed the analysis of elastohydrodynamic theory of line contacts. Das [5] studied the slider bearing lubricated with couple-stress fluids in magnetic field and observed that both the values of the maximum load capacity, and corresponding inlet-outlet film ratio depend on couple stress, magnetic parameters and the shape of bearings. Elsharkawy and Guedouar [6] proposed an efficient numerical scheme to solve the direct lubrication problem for journal bearings lubricated with couple stress fluids, which consists of the modified Reynolds equation, the film thickness equation, and the boundary conditions for the pressure field. Hsu et al. [7] studied the short journal bearings lubricated with the non-Newtonian fluid which is combined with the effects of couple-stresses and surface roughness. It was found that the combined effects of couple stress and surface roughness can improve the load-carrying capacity and decrease the attitude angle and friction parameters. Lahmar [8] also found that the lubricants with couple stress would increase the load-carrying capacity and stability and decrease the friction factor and the attitude angle. The above researches are all about the applications of the couple-stress fluids, and all the results of their studies emphasized that the couple-stress fluids are more superior and more stable than the traditional Newtonian fluids. Chang-Jian and Chen [9] found couple-stress fluid can be used to suppress nonperiodic or even chaotic dynamic response especially for higher rotating speeds in rotor-bearing systems.

Gears have played important roles in power transmission, and therefore the study of gear dynamics is necessary. Many studies have focused on analyzing gear dynamics or relative researches. Vedmar and Andersson [10] presented a method to calculate dynamic gear tooth force and bearing forces and the bearing model was under elastic bearings assumption. The simulation results of elastic model were somewhat different comparing with stiff one. The gear mesh model used with constant was studied by a lot of people, such as Kahraman and Singh [11], Lin et al. [12], Yoon and Rao [13], and Ichimaru and Hirano [14]. Amabili and Fregolent [15] introduced a method based on the measurement of the gear torsional vibrations to identify natural frequency, damping parameters, and equivalent gear error of a spur-gear-pair model. Özgüven and Houser [16, 17] performed dynamic analysis on gears with the effects of variable mesh stiffness, damping, gear errors profile modification, and backlash. Cai and Hayashi [18] calculated the optimum profile modification to obtain a zero vibration of the gear pair. Umezawa et al. [19] analyzed a single DOF numerical gear pair model and compared their numerical results with experimental dynamic transmission errors. McFadden and Toozhy [20] used the high-frequency technique combined with synchronous averaging to detect the failure in rolling element bearings. Litvin et al. [21] proposed a modified geometry of an asymmetric spur-gear drive designed as a favorable shape of transmission errors of reduced magnitude and also reduced contact and bending stresses for an asymmetric spur-gear drive. Guan et al. [22] performed finite-element method to simulate the geared rotor system constructed from beam and lumped mass/stiffness elements and compared the required actuation effort, control robustness, and implementation cost. Giagopoulos et al. [23] presented an analysis on the nonlinear dynamics of a gear-pair system supported on rolling element bearings and used a suitable genetic algorithm to measure noise and model error. Theodossiades and Natsiavas [24] investigated dynamic responses and stability characteristics of rotordynamic systems interconnected

with gear pairs, supported on oil journal bearings. They found many nonperiodic dynamic behaviors. They [25] also analyzed the motor-driven gear-pair systems with backlash and found periodic and chaotic dynamics in this system.

Although virtually all physical phenomena in the real world can be regarded as nonlinear, most of these phenomena can be simplified to a linear form given a sufficiently precise linearization technique. However, this simplification is inappropriate for high-power, high-rotational-speed gear system, and its application during the design and analysis stage may result in a flawed or potentially dangerous operation. As a result, nonlinear analysis methods are generally preferred within engineering and academic circles. The current study performs a nonlinear analysis of the dynamic behavior of a gear-pair system equipped with couple-stress fluid lubricated journal bearings under nonlinear suspension. The nondimensional equation of the gear-bearing system is then solved using the Runge-Kutta method. The nonperiodic behavior of this system is characterized by using phase diagrams, power spectra, Poincaré maps, bifurcation diagrams, Lyapunov exponents, and the fractal dimension of the system.

## 2. Mathematical Modeling

### 2.1. Nonlinear Dynamic Models

Some assumptions are presented to simplify dynamic models to be able to simulate the gear-bearing system, that is, nonlinear suspension (hard spring effect), short journal bearing, nonlinear gear meshing force, and nonlinear couple-stress fluid film force effect are established. Figure 1 shows the gear-bearing model presented in this study. The equations of motion used to describe geometric centers of gear and pinion ( $O_g(X_g, Y_g)$  and  $O_p(X_p, Y_p)$ ) can be written as

$$\begin{aligned} m_p \ddot{X}_p + C \dot{X}_p + K(X_p - X_{j1}) &= W_{cx}, \\ m_p \ddot{Y}_p + C \dot{Y}_p + K(Y_p - Y_{j1}) &= L_{py} - G_{py} - W_{cy} - m_p g, \\ m_g \ddot{X}_g + C \dot{X}_g + K(X_g - X_{jg}) &= -W_{cx}, \\ m_g \ddot{Y}_g + C \dot{Y}_g + K(Y_g - Y_{j2}) &= L_{py} - G_{py} + W_{cy} - m_g g, \end{aligned} \quad (2.1)$$

where  $L_{py}$  and  $L_{gy}$  are the centrifugal forces in the vertical gear mesh direction for pinion and gear,  $G_{py}$  and  $G_{gy}$  are the inertia forces in the vertical gear mesh direction for pinion and gear,  $W_{cx}$  is the dynamic gear mesh force in the horizontal direction, and  $W_{cy}$  is the dynamic gear mesh force in the vertical direction.

The equations of motion of the center of bearing 1 ( $X_1, Y_1$ ) and the center of bearing 2 ( $X_2, Y_2$ ) under the assumption of nonlinear suspension can be written as

$$\begin{aligned} m_1 \ddot{X}_1 + c_1 \dot{X}_1 + k_{11} X_1 + k_{12} X_1^3 &= F_{x1}, \\ m_1 \ddot{Y}_1 + c_1 \dot{Y}_1 + k_{11} Y_1 + k_{12} Y_1^3 &= -m_1 g + F_{y1}, \\ m_2 \ddot{X}_2 + c_2 \dot{X}_2 + k_{21} X_2 + k_{22} X_2^3 &= F_{x2}, \\ m_2 \ddot{Y}_2 + c_2 \dot{Y}_2 + k_{21} Y_2 + k_{22} Y_2^3 &= -m_2 g + F_{y2}. \end{aligned} \quad (2.2)$$

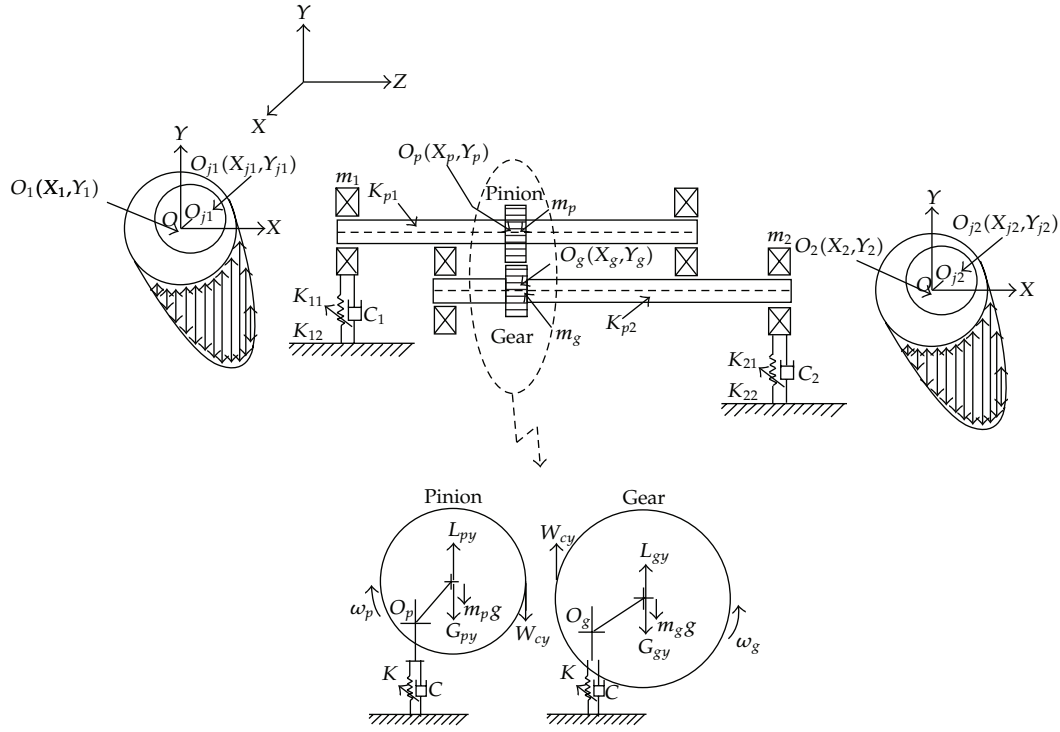


**Figure 1:** Schematic illustration of the gear-bearing system under nonlinear suspension and the model of force diagram for pinion and gear.

According to the principles of force equilibrium, the forces acting at the center of journal 1, that is,  $O_{j1}(X_{j1}, Y_{j1})$  and center of journal 2, that is,  $O_{j2}(X_{j2}, Y_{j2})$  are given by

$$\begin{aligned}
 F_{x1} &= f_{e1} \cos \varphi_1 + f_{\varphi 1} \sin \varphi_1 = \frac{K_{p1}(X_p - X_{j1})}{2}, \\
 F_{y1} &= f_{e1} \sin \varphi_1 - f_{\varphi 1} \cos \varphi_1 = \frac{K_{p1}(Y_p - Y_{j1})}{2}, \\
 F_{x2} &= f_{e2} \cos \varphi_2 + f_{\varphi 2} \sin \varphi_2 = \frac{K_{p2}(X_g - X_{j2})}{2}, \\
 F_{y2} &= f_{e2} \sin \varphi_2 - f_{\varphi 2} \cos \varphi_2 = \frac{K_{p2}(Y_g - Y_{j2})}{2},
 \end{aligned} \tag{2.3}$$

in which  $f_{e1}$  and  $f_{\varphi 1}$  are the viscous damping forces in the radial and tangential directions for the center of journal 1, respectively, and  $f_{e2}$  and  $f_{\varphi 2}$  are the viscous damping forces in the radial and tangential directions for the center of journal 2, respectively.

## 2.2. Nonlinear Couple-Stress Fluid Film Force

The non-Newtonian Reynolds-type equation can be performed as

$$\frac{\partial}{\partial x} \left( g(h, l) \frac{\partial p}{\partial x} \right) + \frac{\partial}{\partial z} \left( g(h, l) \frac{\partial p}{\partial z} \right) = 6 \mu U \frac{\partial h}{\partial x} + 12 \mu \frac{\partial h}{\partial t}, \quad (2.4)$$

where  $g(h, l) = h^3 - 12l^2 h + 24l^3 \tan h(h/2l)$ ,  $\partial h / \partial x = -(c\varepsilon/R) \sin \theta$ ,  $\partial h / \partial t = c\dot{\varepsilon} \cos \theta + c\varepsilon\dot{\varphi} \sin \theta$ ,  $x = R\theta$ ,  $U = R\omega$ ,  $\varepsilon = e/c$ , and  $h = c(1 + \varepsilon \cos(\gamma - \varphi(t))) = c(1 + \varepsilon \cos \theta)$ . Thus  $g(h, l)$  can also be performed as  $g(h, l) = c^3(1 + \varepsilon \cos \theta)^3 - 12l^2 c(1 + \varepsilon \cos \theta) + 24l^3 \tan h(c(1 + \varepsilon \cos \theta)/2l)$ , where  $l = (\eta/\mu)^{1/2}$ , in which  $\mu$  is the classical viscosity parameter and  $\eta$  is a new material constant peculiar to fluids with couple stresses and Reynolds equation that can be rewritten as

$$\frac{\partial}{R\partial\theta} \left( g(h, l) \frac{\partial p}{R\partial\theta} \right) + \frac{\partial}{\partial z} \left( g(h, l) \frac{\partial p}{\partial z} \right) = -6 \mu \omega c \varepsilon \sin \theta + 12 \mu (c\dot{\varepsilon} \cos \theta + c\varepsilon\dot{\varphi} \sin \theta). \quad (2.5)$$

Using the “short bearing approximation” ( $L/D < 0.25$ ,  $\partial p / \partial \theta \ll \partial p / \partial z$ ), then we can set  $\partial p / \partial \theta = 0$ . The following equation can be introduced:

$$\frac{\partial^2 p}{\partial z^2} = \frac{-6 \mu \omega c \varepsilon \sin \theta + 12 \mu (c\dot{\varepsilon} \cos \theta + c\varepsilon\dot{\varphi} \sin \theta)}{g(h, l)}. \quad (2.6)$$

The resulting damping forces about the journal center in the radial and tangential directions are determined by integrating pressure distribution over the area of the journal sleeve:

$$f_e = F \cos \varphi = \int_0^L r \int_0^{2\pi} p(\theta) \cos \theta d\theta dz, \quad (2.7)$$

$$f_\varphi = F \sin \varphi = \int_0^L r \int_0^{2\pi} p(\theta) \sin \theta d\theta dz. \quad (2.8)$$

Substituting (2.7) and (2.8) into (2.2)–(2.3) enables the values of  $F_{x1}$ ,  $F_{x2}$ ,  $F_{y1}$ , and  $F_{y2}$  to be obtained.

## 2.3. Nonlinear Gear Meshing Force

Figure 2 presents a schematic illustration of the dynamic model considered between gear and pinion.  $L_{py}$  and  $L_{gy}$  are the centrifugal forces in the vertical gear mesh direction for pinion and gear,  $G_{py}$  and  $G_{gy}$  are the inertia forces in the vertical gear mesh direction for pinion and gear,  $W_{cx}$  is the dynamic gear mesh force in the horizontal direction, and  $W_{cy}$  is the dynamic gear

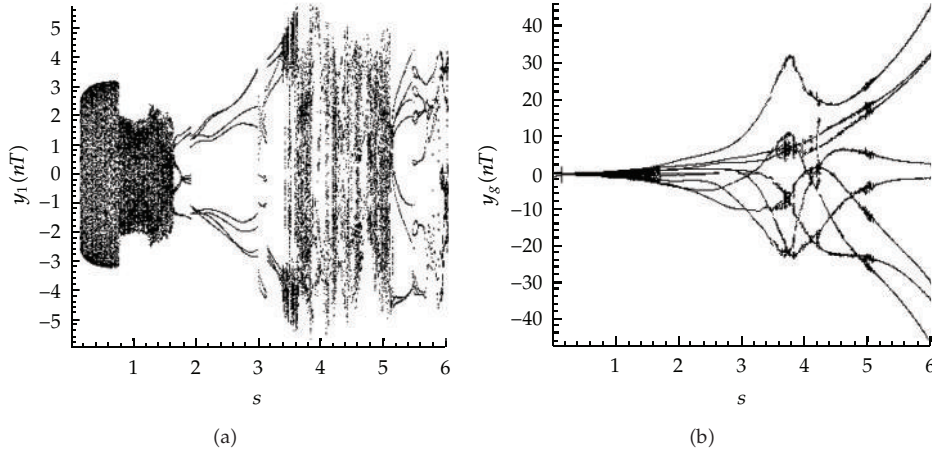


**Figure 2:** Bifurcation diagrams of gear-bearing system using dimensionless rotational speed ratio,  $s$ , as bifurcation parameter for non-Newtonian lubricating fluid with  $l^* = 0.0$ .

mesh force in the vertical direction. Thus,  $L_{py}$ ,  $L_{gy}$ ,  $G_{py}$ ,  $G_{gy}$ ,  $W_{cx}$ , and  $W_{cy}$  can be performed as

$$\begin{aligned}
 L_{py} &= m_p e_p \omega_p^2 \sin \theta_1, \\
 L_{gy} &= m_g e_g \omega_g^2 \sin \theta_2, \\
 G_{py} &= m_p e_p \ddot{\theta}_1 \cos \theta_1, \\
 G_{gy} &= m_g e_g \ddot{\theta}_2 \cos \theta_2, \\
 W_{cx} &= C_m (\dot{X}_p - \dot{X}_g - e_p \Omega \sin(\Omega t)) + K_m (X_p - X_g - e_p \cos(\Omega t)), \\
 W_{cy} &= C_m (\dot{Y}_p - \dot{Y}_g - e_p \Omega \cos(\Omega t)) + K_m (Y_p - Y_g - e_p \sin(\Omega t)).
 \end{aligned} \tag{2.9}$$

Substituting (2.9) into (2.1) enables the values of  $L_{py}$ ,  $L_{gy}$ ,  $G_{py}$ ,  $G_{gy}$ ,  $W_{cx}$ , and  $W_{cy}$  to be obtained.

#### 2.4. Dimensionless of Nonlinear Dynamic Models

Couple-stress fluid film force and gear meshing force would be introduced in Equations (2.1)–(2.3) and can be nondimensionalized to yield the following equations:

$$\begin{aligned}
 \varepsilon'_1 &= \frac{\beta_1 c K_p [(y_p - y_1 - \varepsilon_1 \sin \varphi_1) \cos \varphi_1 - (x_p - x_1 - \varepsilon_1 \cos \varphi_1) \sin \varphi_1]}{4\alpha_1 (\gamma_1 \delta_1 - \beta_1^2) \omega} \\
 &\quad - \frac{\delta_1 c K_p [(x_p - x_1 - \varepsilon_1 \cos \varphi_1) \cos \varphi_1 + (y_p - y_1 - \varepsilon_1 \sin \varphi_1) \sin \varphi_1]}{4\alpha_1 (\gamma_1 \delta_1 - \beta_1^2) \omega},
 \end{aligned}$$

$$\varphi_1' = \frac{1}{2} - \frac{cK_p [(y_p - y_1 - \varepsilon_1 \sin \varphi_1) \cos \varphi_1 - (x_p - x_1 - \varepsilon_1 \cos \varphi_1) \sin \varphi_1]}{4\alpha_1 \delta_1 \varepsilon_1 \omega}$$

$$- \left( \frac{\beta_1^2 cK_p [(y_p - y_1 - \varepsilon_1 \sin \varphi_1) \cos \varphi_1 - (x_p - x_1 - \varepsilon_1 \cos \varphi_1) \sin \varphi_1]}{4\alpha_1 \varepsilon_1 \delta_1 (\gamma_1 \delta_1 - \beta_1^2) \omega} \right.$$

$$\left. - \frac{\beta_1 \delta_1 cK_p [(x_p - x_1 - \varepsilon_1 \cos \varphi_1) \cos \varphi_1 + (y_p - y_1 - \varepsilon_1 \sin \varphi_1) \sin \varphi_1]}{4\alpha_1 \varepsilon_1 \delta_1 (\gamma_1 \delta_1 - \beta_1^2) \omega} \right),$$

$$\varepsilon_2' = \frac{\beta_2 cK_p [(y_g - y_2 - \varepsilon_2 \sin \varphi_2) \cos \varphi_2 - (x_g - x_2 - \varepsilon_2 \cos \varphi_2) \sin \varphi_2]}{4\alpha_2 (\gamma_2 \delta_2 - \beta_2^2) \omega}$$

$$- \frac{\delta_2 cK_p [(x_g - x_2 - \varepsilon_2 \cos \varphi_2) \cos \varphi_2 + (y_g - y_2 - \varepsilon_2 \sin \varphi_2) \sin \varphi_2]}{4\alpha_2 (\gamma_2 \delta_2 - \beta_2^2) \omega},$$

$$\varphi_2' = \frac{1}{2} - \frac{cK_p [(y_g - y_2 - \varepsilon_2 \sin \varphi_2) \cos \varphi_2 - (x_g - x_2 - \varepsilon_2 \cos \varphi_2) \sin \varphi_2]}{4\alpha_2 \delta_2 \varepsilon_2 \omega}$$

$$- \left( \frac{\beta_2^2 cK_p [(y_g - y_2 - \varepsilon_2 \sin \varphi_2) \cos \varphi_2 - (x_g - x_2 - \varepsilon_2 \cos \varphi_2) \sin \varphi_2]}{4\alpha_2 \varepsilon_2 \delta_2 (\gamma_2 \delta_2 - \beta_2^2) \omega} \right.$$

$$\left. - \frac{\beta_2 \delta_2 cK_p [(x_g - x_2 - \varepsilon_2 \cos \varphi_2) \cos \varphi_2 + (y_g - y_2 - \varepsilon_2 \sin \varphi_2) \sin \varphi_2]}{4\alpha_2 \varepsilon_2 \delta_2 (\gamma_2 \delta_2 - \beta_2^2) \omega} \right),$$

$$x_p'' = -\frac{2\xi_2}{s} x_p' - \frac{1}{s^2} (x_p - x_1 - \varepsilon_1 \cos \varphi_1) + \beta \cos\left(\frac{\phi}{4}\right) - \frac{2\xi_3}{s} (x_p' - x_g' - E_p \sin \phi)$$

$$- \frac{\Lambda}{s^2} (x_p - x_g - E_p \cos \phi),$$

$$y_p'' = -\frac{2\xi_2}{s} y_p' - \frac{1}{s^2} (y_p - y_1 - \varepsilon_1 \sin \varphi_1) + \beta \sin\left(\frac{\phi}{4}\right) - \frac{2\xi_3}{s} (y_p' - y_g' - E_p \cos \phi)$$

$$- \frac{\Lambda}{s^2} (y_p - y_g - E_p \sin \phi) - \frac{f}{s^2},$$

$$x_g'' = -\frac{2\xi_4}{s} x_g' - \frac{1}{s^2} (x_g - x_2 - \varepsilon_2 \cos \varphi_2) + \beta_g \cos\left(\frac{\phi}{8}\right) + \frac{2\xi_5}{s} (x_p' - x_g' - E_p \sin \phi)$$

$$- \frac{\Lambda_g}{s^2} (x_p - x_g - E_p \cos \phi),$$

$$y_g'' = -\frac{2\xi_4}{s} y_g' - \frac{1}{s^2} (y_g - y_2 - \varepsilon_2 \sin \varphi_2) + \beta_g \sin\left(\frac{\phi}{8}\right) + \frac{2\xi_5}{s} (y_p' - y_g' - E_p \cos \phi)$$

$$+ \frac{\Lambda_g}{s^2} (y_p - y_g - E_p \sin \phi) - \frac{f_g}{s^2},$$

$$\begin{aligned}
x_1'' + \frac{2\xi_1}{s_1}x_1' + \frac{1}{s_1^2}x_1 + \frac{\alpha_1}{s_1^2}x_1^3 - \frac{1}{2C_{1p}s^2}(x_p - x_1 - \varepsilon_1 \cos \varphi_1) &= 0, \\
y_1'' + \frac{2\xi_1}{s_1}y_1' + \frac{1}{s_1^2}y_1 + \frac{\alpha_1}{s_1^2}y_1^3 - \frac{1}{2C_{om}s^2}(y_p - y_1 - \varepsilon_1 \sin \varphi_1) + \frac{f}{s^2} &= 0, \\
x_2'' + \frac{2\xi_6}{s_2}x_2' + \frac{1}{s_2^2}x_2 + \frac{\alpha_2}{s_2^2}x_2^3 - \frac{1}{2C_{2p}s^2}(x_g - x_2 - \varepsilon_2 \cos \varphi_2) &= 0, \\
y_2'' + \frac{2\xi_6}{s_2}y_2' + \frac{1}{s_2^2}y_2 + \frac{\alpha_2}{s_2^2}y_2^3 - \frac{1}{2C_{2p}s^2}(y_g - y_2 - \varepsilon_2 \sin \varphi_2) + \frac{f}{s^2} &= 0,
\end{aligned} \tag{2.10}$$

where

$$\begin{aligned}
\alpha_1 &= -\frac{\mu L^3 R}{2c^2}, \\
\beta_1 &= \int_0^\pi \frac{\sin \theta \cos \theta}{\left[ (1 + \varepsilon_1 \cos \theta)^3 - 12(l^*)^2(1 + \varepsilon_1 \cos \theta) + 24(l^*)^3 \tanh((1 + \varepsilon_1 \cos \theta)/2l^*) \right]} d\theta, \\
\gamma_1 &= \int_0^\pi \frac{\cos^2 \theta}{\left[ (1 + \varepsilon_1 \cos \theta)^3 - 12(l^*)^2(1 + \varepsilon_1 \cos \theta) + 24(l^*)^3 \tanh((1 + \varepsilon_1 \cos \theta)/2l^*) \right]} d\theta, \\
\delta_1 &= \int_0^\pi \frac{\sin^2 \theta}{\left[ (1 + \varepsilon_1 \cos \theta)^3 - 12(l^*)^2(1 + \varepsilon_1 \cos \theta) + 24(l^*)^3 \tanh((1 + \varepsilon_1 \cos \theta)/2l^*) \right]} d\theta, \\
\alpha_2 &= -\frac{\mu L^3 R}{2c^2}, \\
\beta_2 &= \int_0^\pi \frac{\sin \theta \cos \theta}{\left[ (1 + \varepsilon_2 \cos \theta)^3 - 12(l^*)^2(1 + \varepsilon_2 \cos \theta) + 24(l^*)^3 \tanh((1 + \varepsilon_2 \cos \theta)/2l^*) \right]} d\theta, \\
\gamma_2 &= \int_0^\pi \frac{\cos^2 \theta}{\left[ (1 + \varepsilon_2 \cos \theta)^3 - 12(l^*)^2(1 + \varepsilon_2 \cos \theta) + 24(l^*)^3 \tanh((1 + \varepsilon_2 \cos \theta)/2l^*) \right]} d\theta, \\
\delta_2 &= \int_0^\pi \frac{\sin^2 \theta}{\left[ (1 + \varepsilon_2 \cos \theta)^3 - 12(l^*)^2(1 + \varepsilon_2 \cos \theta) + 24(l^*)^3 \tanh((1 + \varepsilon_2 \cos \theta)/2l^*) \right]} d\theta,
\end{aligned} \tag{2.11}$$

where  $l^* = l/c$  is the dimensionless parameter for  $l$ .

Equation (2.10) describes a nonlinear dynamic system. In the current study, the approximate solutions of these coupled non-linear differential equations are obtained using the fourth-order Runge-Kutta numerical scheme.

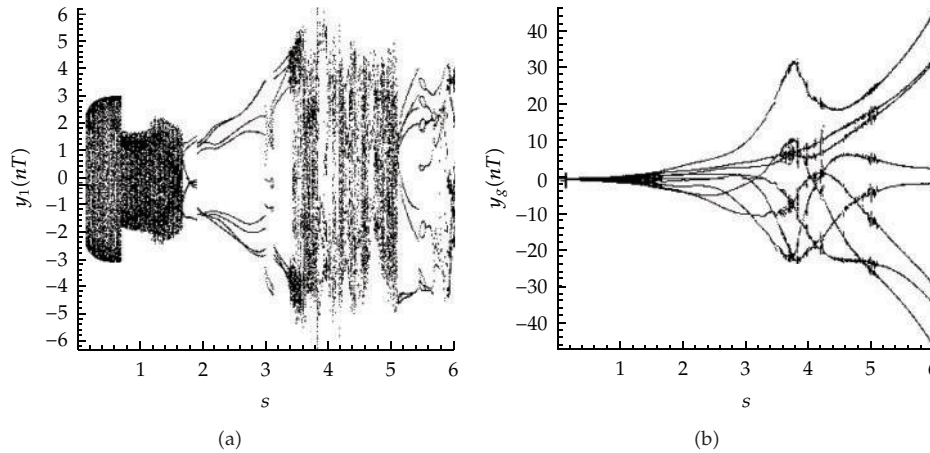


**Figure 3:** Bifurcation diagrams of gear-bearing system using dimensionless rotational speed ratio,  $s$ , as bifurcation parameter for non-Newtonian lubricating fluid with  $l^* = 0.1$ .

### 3. Analytical Tools for Observing Nonlinear Dynamics of Gear-Bearing System

In the present study, the nonlinear dynamics of the gear-bearing system shown in Figure 1 are analyzed using Poincaré maps, bifurcation diagrams, Lyapunov exponent, and fractal dimension. The dynamic trajectories of the gear-bearing system provide a basic indication as to whether the system behavior is periodic or nonperiodic. The projection of the Poincaré section on the  $y(nT)$  plane is referred to as the Poincaré map of the dynamic system. When the system performs quasiperiodic motion, the return points in the Poincaré map form a closed curve. For chaotic motion, the return points form a fractal structure comprising many irregularly distributed points. Finally, for  $nT$ -periodic motion, the return points have the form of  $n$  discrete points. In this study, the spectrum components of the motion performed by the gear-bearing system are analyzed by using the Fast Fourier Transformation method to derive the power spectrum of the displacement of the dimensionless dynamic transmission error. In the analysis, the frequency axis of the power spectrum plot is normalized using the rotational speed,  $\omega$ .

A bifurcation diagram summarizes the essential dynamics of a gear-train system and is therefore a useful means of observing its nonlinear dynamic response. In the present analysis, the bifurcation diagrams are generated using the dimensionless rotational speed ratio,  $s$ , to be a control parameter. In each case, the bifurcation control parameter is varied with a constant step and the state variables at the end of one integration step are taken as the initial values for the next step. The corresponding variations of the  $y(nT)$  coordinates of the return points in the Poincaré map are then plotted to form the bifurcation diagram.

The Lyapunov exponent of a dynamic system characterizes the rate of separation of infinitesimally close trajectories and provides a useful test for the presence of chaos. In a chaotic system, the points of nearby trajectories starting initially within a sphere of radius  $\varepsilon_0$  form after time  $t$  an approximately ellipsoidal distribution with semiaxes of length  $\varepsilon_j(t)$ . The Lyapunov exponents of a dynamic system are defined by  $\lambda_j = \lim_{t \rightarrow \infty} (1/t) \log(\varepsilon_j(t)/\varepsilon_0)$ , where  $\lambda_j$  denotes the rate of divergence of the nearby trajectories. The exponents of a system

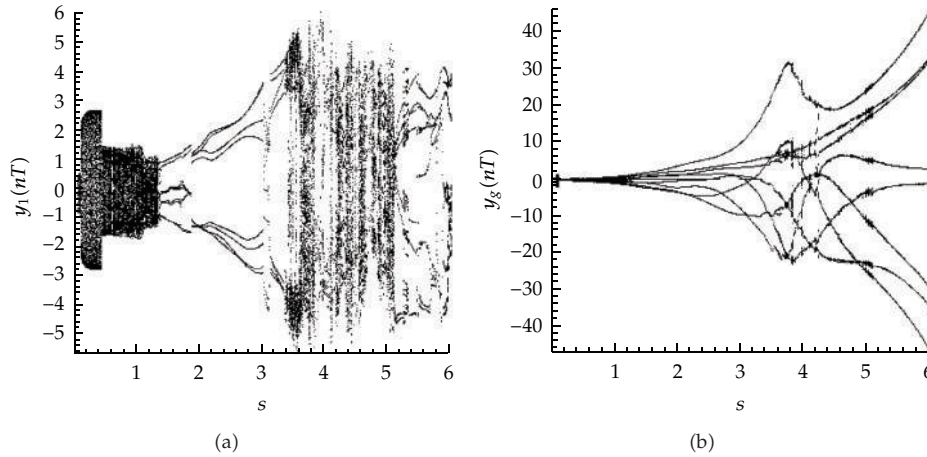


**Figure 4:** Bifurcation diagrams of gear-bearing system using dimensionless rotational speed ratio,  $s$ , as bifurcation parameter for non-Newtonian lubricating fluid with  $l^* = 0.3$ .

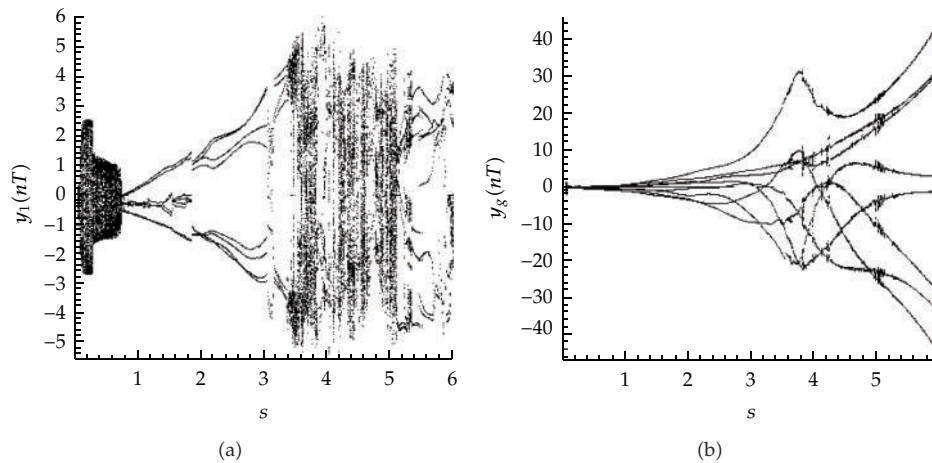


**Figure 5:** Bifurcation diagrams of gear-bearing system using dimensionless rotational speed ratio,  $s$ , as bifurcation parameter for non-Newtonian lubricating fluid with  $l^* = 0.5$ .

are usually ordered into a Lyapunov spectrum, that is,  $\lambda_1 > \lambda_2 > \dots > \lambda_m$ . A positive value of the maximum Lyapunov exponent ( $\lambda_1$ ) is generally taken as an indication of chaotic motion.

The presence of chaotic vibration in a system is generally detected using either the Lyapunov exponent or the fractal dimension property. The Lyapunov exponent test can be used for both dissipative systems and nondissipative (i.e., conservative) systems, but it is not easily applied to the analysis of experimental data. Conversely, the fractal dimension test can only be used for dissipative systems, but it is easily applied to experimental data. In contrast to Fourier transform-based techniques and bifurcation diagrams, which provide only a general indication of the change from periodic motion to chaotic behavior, dimensional measures allow chaotic signals to be differentiated from random signals. Although many dimensional measures have been proposed, the most commonly applied measure is the

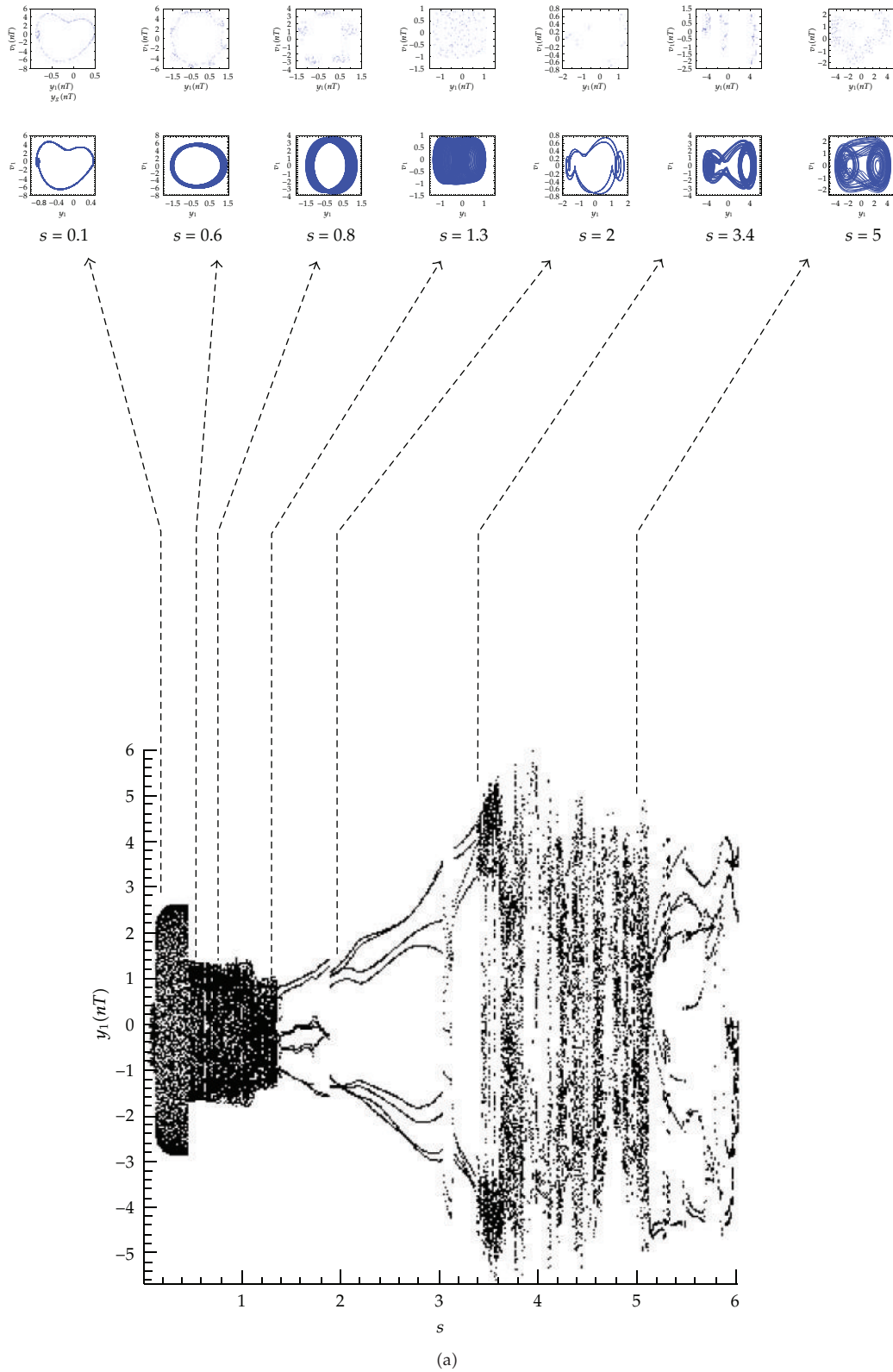
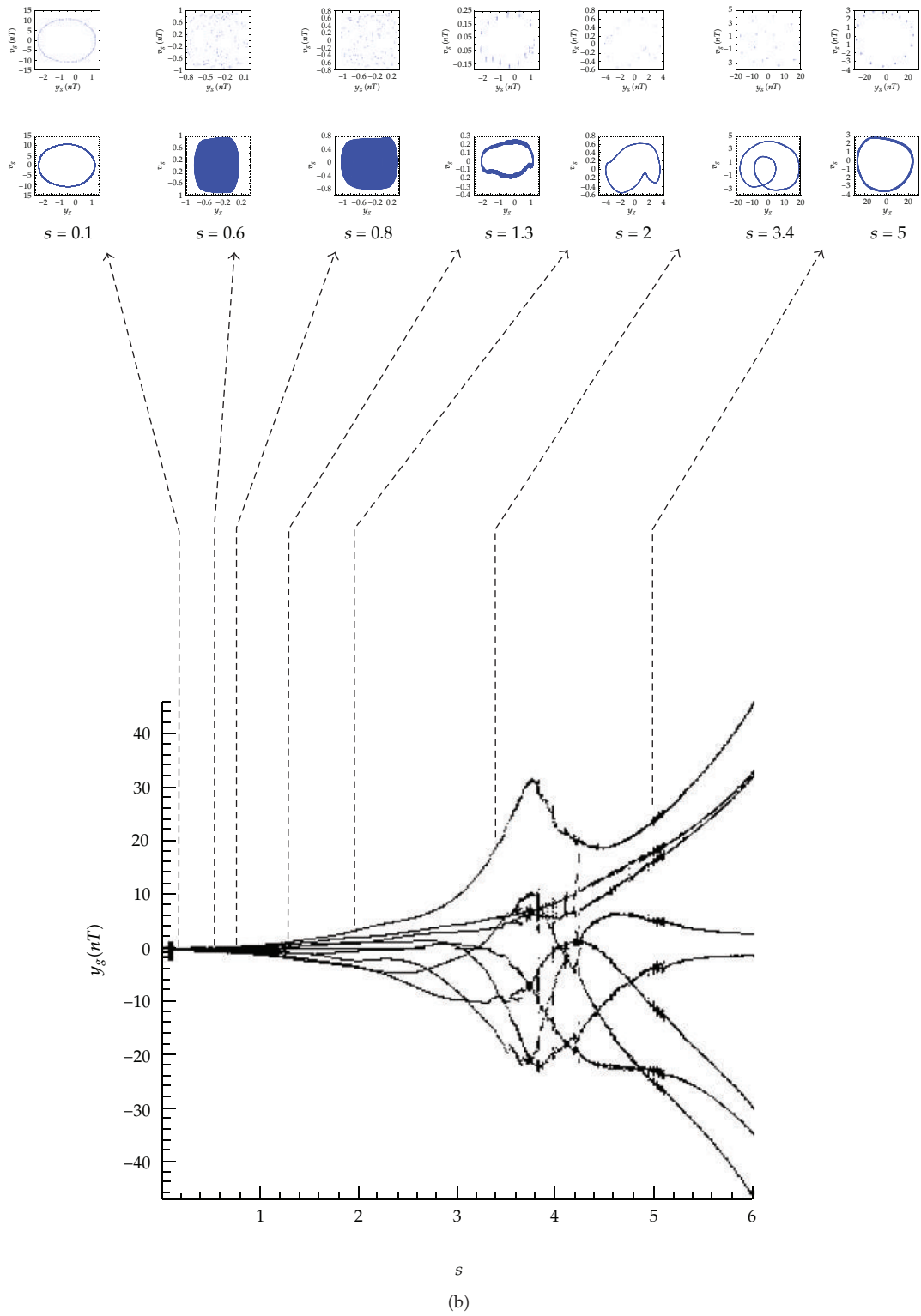


Figure 6: Continued.



**Figure 6:** Bifurcation diagrams of gear-bearing system using dimensionless rotational speed ratio,  $s$ , as bifurcation parameter for non-Newtonian lubricating fluid with  $l^* = 0.3$ .

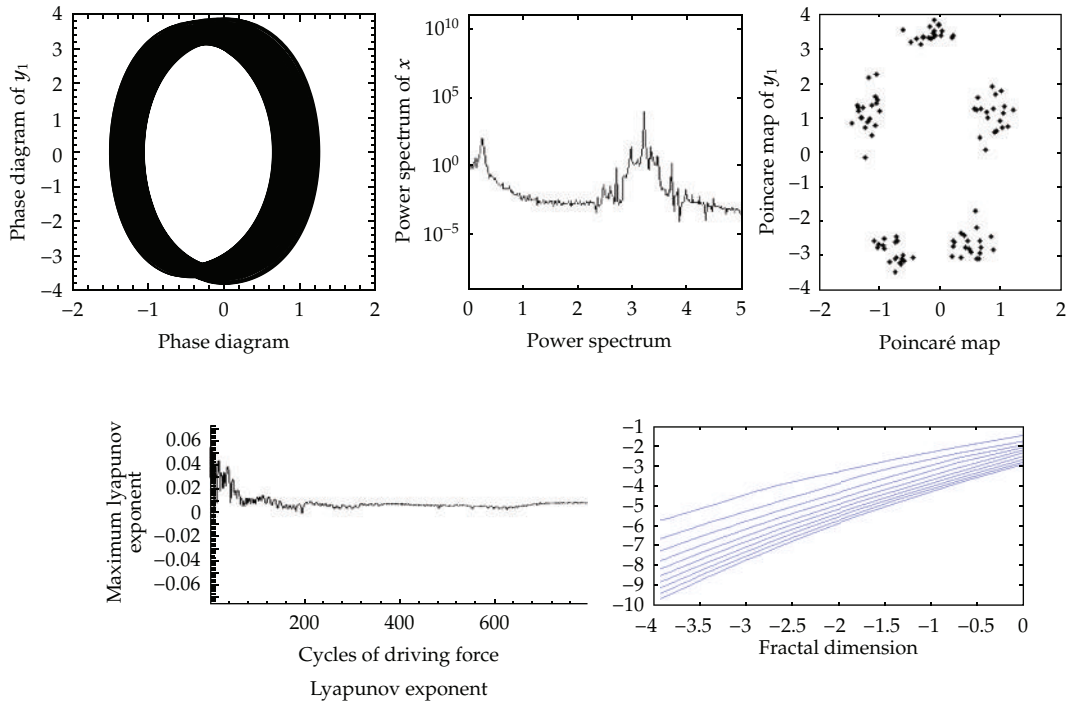


Figure 7: Simulation results obtained for gear-bearing system with  $s = 0.8$  for  $y_1$  ( $l^* = 0.3$ ).

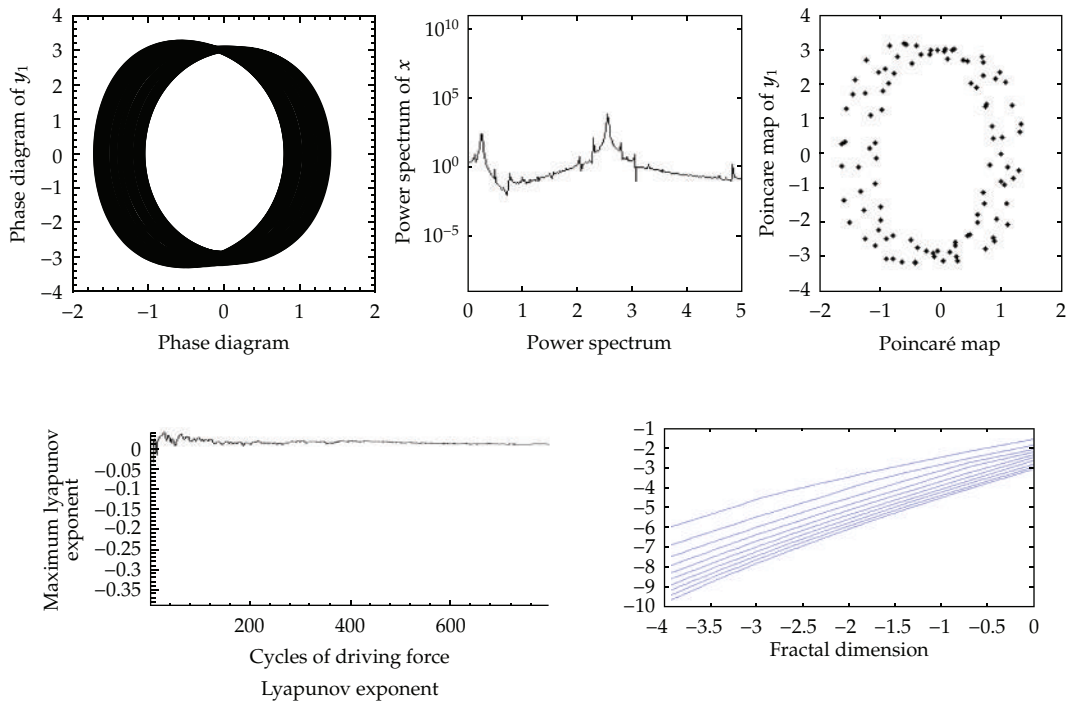
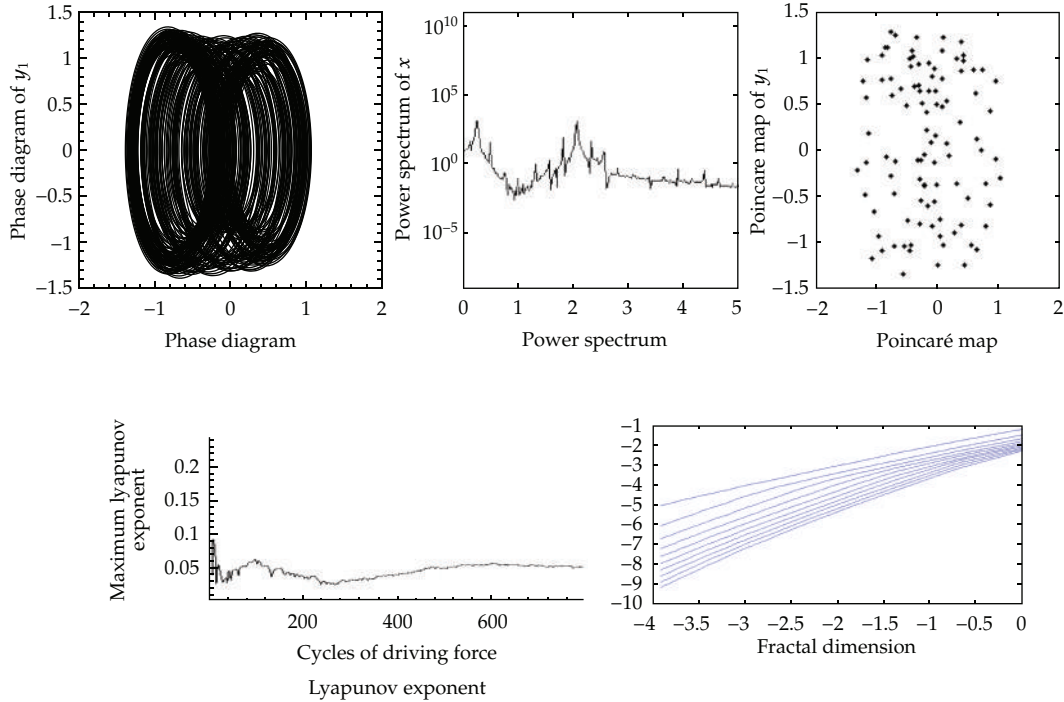


Figure 8: Simulation results obtained for gear-bearing system with  $s = 1.0$  for  $y_1$  ( $l^* = 0.3$ ).



**Figure 9:** Simulation results obtained for gear-bearing system with  $s = 4.2$  for  $y_1$  ( $l^* = 0.3$ ).

correlation dimension  $d_G$  defined by Grassberger and Procaccia due to its computational speed and the consistency of its results. However, before the correlation dimension of a dynamic system flow can be evaluated, it is first necessary to generate a time series of one of the system variables using a time-delayed pseudo-phase-plane method. Assume an original time series of  $x_i = \{x(i\tau); i = 1, 2, 3, \dots, N\}$ , where  $\tau$  is the time delay (or sampling time). If the system is acted upon by an excitation force with a frequency  $\omega$ , the sampling time,  $\tau$ , is generally chosen such that it is much smaller than the driving period. The delay coordinates are then used to construct an  $n$ -dimensional vector  $X = (x(j\tau), x[(j+1)\tau], x[(j+2)\tau], \dots, x[(j+n-1)\tau])$ , where  $j = 1, 2, 3, \dots, (N-n+1)$ . The resulting vector comprises a total of  $(N-n+1)$  vectors, which are then plotted in an  $n$ -dimensional embedding space. Importantly, the system flow in the reconstructed  $n$ -dimensional phase space retains the dynamic characteristics of the system in the original phase space. In other words, if the system flow has the form of a closed orbit in the original phase plane, it also forms a closed path in the  $n$ -dimensional embedding space. Similarly, if the system exhibits a chaotic behavior in the original phase plane, its path in the embedding space will also be chaotic. The characteristics of the attractor in the  $n$ -dimensional embedding space are generally tested using the function  $\sum_{i,j=1}^N H(r - |x_i - x_j|)$  to determine the number of pairs  $(i, j)$  lying within a distance  $|x_i - x_j| < r$  in  $\{x_i\}_{i=1}^N$ , where  $H$  denotes the Heaviside step function,  $N$  represents the number of data points, and  $r$  is the radius of an  $n$ -dimensional hyper-sphere. For many attractors, this function exhibits a power law dependence on  $r$  as  $r \rightarrow 0$ , that is,  $c(r) \propto r^{d_G}$ . Therefore, the correlation dimension,  $d_G$ , can be determined from the slope of a plot of  $[\log c(r)]$  versus  $[\log r]$ . Grassberger and Procaccia [26] showed that the correlation dimension represents the lower bound to the capacity or fractal dimension  $d_c$  and approaches its value asymptotically

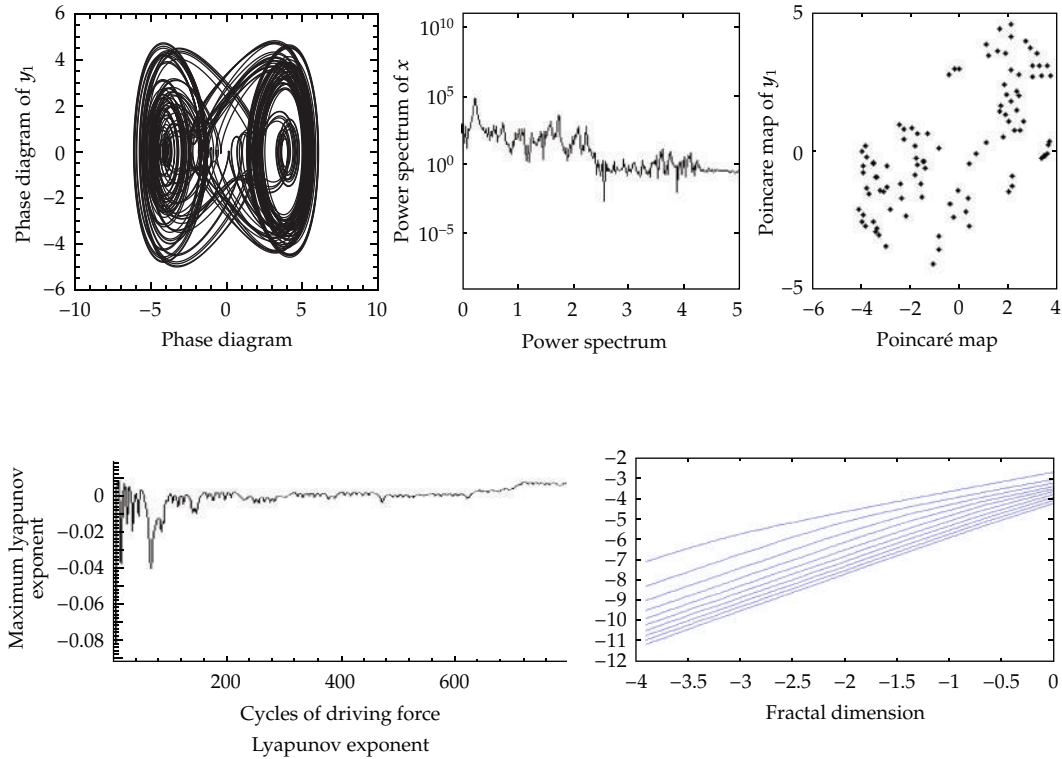
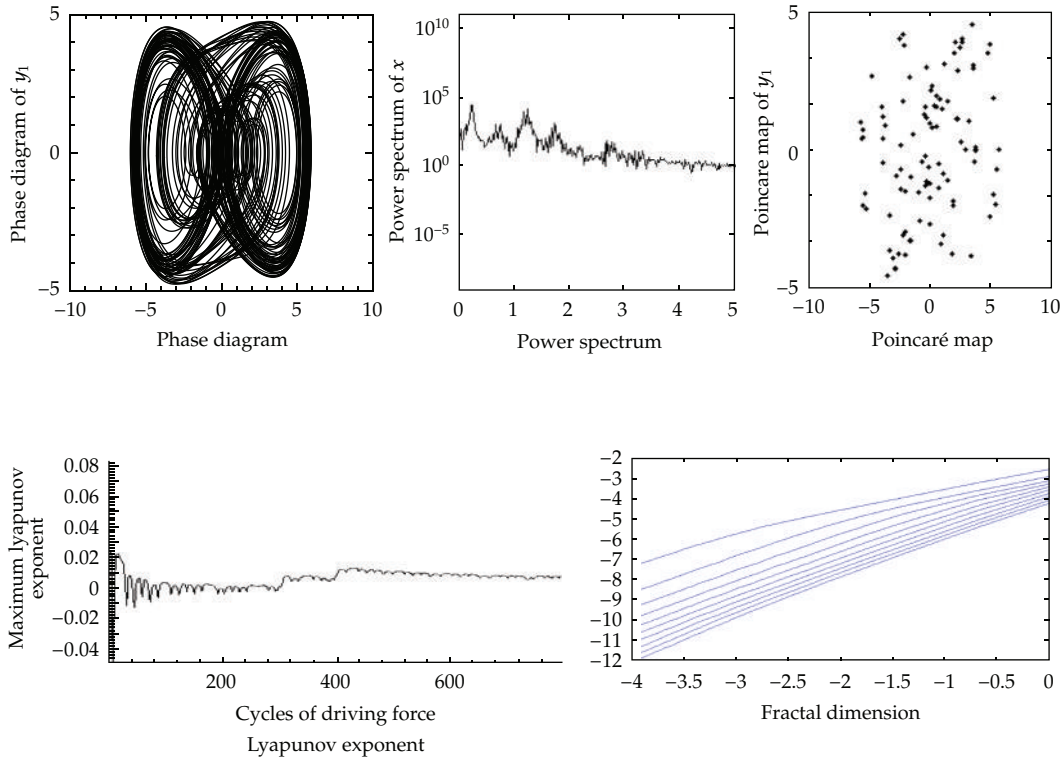


Figure 10: Simulation results obtained for gear-bearing system with  $s = 5.0$  for  $y_1$  ( $l^* = 0.3$ ).

when the attracting set is distributed more uniformly in the embedding phase space. A set of points in the embedding space is said to be fractal if its dimension has a finite noninteger value. Otherwise, the attractor is referred to as a “strange attractor.” To establish the nature of the attractor, the embedding dimension is progressively increased, causing the slope of the characteristic curve to approach a steady-state value. This value is then used to determine whether the system has a fractal structure or a strange attractor structure. If the dimension of the system flow is found to be fractal (i.e., to have a noninteger value), the system is judged to be chaotic.

#### 4. Numerical Results and Discussions

The nonlinear dynamic equations presented in (2.10) for the gear-bearing system with nonlinear suspension effects, couple-stress fluid effect, strongly nonlinear oil-film force, and nonlinear gear mesh force were solved using the fourth-order Runge-Kutta method. The time step in the iterative solution procedure was assigned a value of  $\pi/300$  and the termination criterion was specified as an error tolerance of less than 0.0001. The time series data corresponding to the first 800 revolutions of the two gears were deliberately excluded from the dynamic analysis to ensure that the analyzed data related to steady-state conditions. The sampled data were used to generate the dynamic trajectories, Poincaré maps, and bifurcation diagrams of the spur-gear system in order to obtain a basic understanding of its dynamic behavior. The maximum Lyapunov exponent and the fractal dimension measure



**Figure 11:** Simulation results obtained for gear-bearing system with  $s = 1.2$  for  $y_1$  ( $l^* = 0.3$ ).

were then used to identify the onset of chaotic motion. For convenience, only the data of the displacements in the vertical direction were used to generate diagrams.

The rotational speed ratio  $s$  is commonly used as a control parameter for bifurcation diagrams to analyze nonlinear behaviors of rotor-dynamics, gear-dynamics, bearing systems or machine tools. Accordingly, the dynamic behavior of the current gear-bearing system was examined using the dimensionless rotational speed ratio  $s$  as a bifurcation control parameter. Figures 2, 3, 4 and 5 are the bifurcation diagrams for the gear-bearing system displacement against the dimensionless rotational speed ratio,  $s$ , for non-Newtonian lubricating fluid with  $l^* = 0.0, 0.1, 0.3$ , and  $0.5$  to describe corresponding dynamic responses. It can be observed that the dynamic behaviors of bearing center and gear center show abundant nonperiodic responses at low speeds. The dynamic behaviors become steady and come into subharmonic motions as rotating with high speed but would behave nonperiodic vibrations and higher amplitude for higher rotating speeds (i.e.,  $s > 3.0$ ). It is said that the couple-stress fluid can improve lubricating conditions and therefore can enhance dynamic responses for turbomachineries. According to bifurcation results, we would find dynamic behaviors show different results with different  $l^*$ . When  $l^* = 0.0$ , lubricating fluid as Newtonian fluid and the effect of couple-stress fluid would be greater as  $l^*$  becomes greater. The results show that the range of nonperiodic motions or subharmonic vibrations would be shortened and the amplitude of the systems would also be suppressed as  $l^*$  increases. Nevertheless, higher values of  $l^*$  could not suppress nonperiodic vibrations occurring at high speeds. We also find that the dynamic behaviors of bearing center and gear center are nonsynchronous and the couple-stress fluid can not also improve gear-dynamics as  $l^*$  increases.

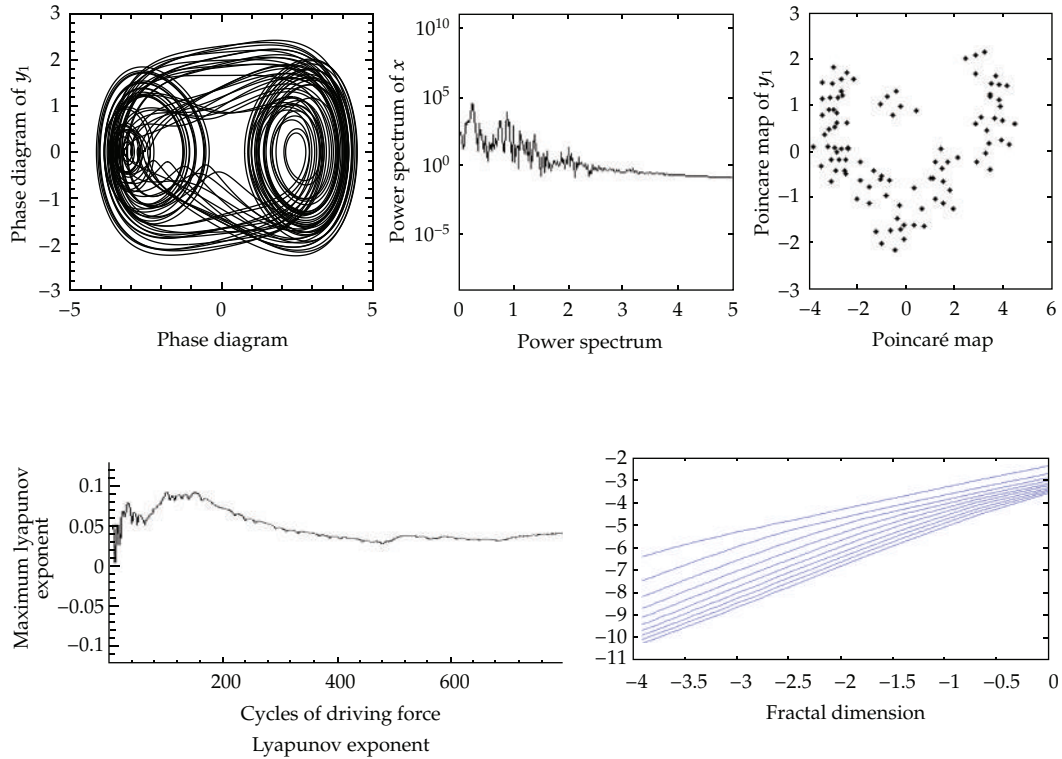


**Figure 12:** Simulation results obtained for gear-bearing system with  $s = 3.6$  for  $y_1$  ( $l^* = 0.3$ ).

Figures 6(a) and 6(b) present the bifurcation diagrams for the gear-bearing system displacement against the dimensionless rotational speed ratio,  $s$ , for non-Newtonian lubricating fluid with  $l^* = 0.3$  and some dynamic trajectories and Poincaré maps (e.g.,  $s = 0.1, 0.6, 0.8, 1.3, 2.0, 3.4,$  and  $5.0$ ) are exemplified to describe corresponding dynamic responses. The bifurcation diagram of bearing center shows quasiperiodic responses at low speeds as  $s < 0.15$  and turns to nonperiodic or even chaotic motions as  $s > 0.15$ . When rotating speed becomes greater ( $s > 1.39$ ), the dynamic responses behave  $nT$ -periodic motions, but dynamic responses of bearing center present strongly nonperiodic motions and the amplitude of the system is also greater than the amplitude of lower rotating speeds. Figures 7, 8, 9, 10, 11, and 12 are simulation results of phase diagrams, power spectra, Poincaré maps, Lyapunov exponent and fractal dimension with  $s = 0.8, 1.0, 1.2, 3.6, 4.2,$  and  $5.0$  for  $y_1$  ( $l^* = 0.3$ ). In the above case, the phase diagrams are highly disordered and the power spectra reveal numerous excitation frequencies. Furthermore, it can be seen that the return points in the Poincaré maps form geometrically fractal structures and the maximum Lyapunov exponent is positive in each case. In other words, the results presented in these figures all indicate that the gear center exhibits a chaotic behavior at those values.

## 5. Conclusions

This study has performed a numerical analysis of the nonlinear dynamic response of a gear-bearing system subject to nonlinear suspension effects, couple-stress fluid effect, nonlinear

oil-film force, and nonlinear gear mesh force. The dynamics of the system have been analyzed by reference to its dynamic trajectories, power spectra, Poincaré maps, bifurcation diagrams, maximum Lyapunov exponents, and fractal dimensions. When rotating machineries are turned on, they must meet low rotating speeds and according to the results shown in the bifurcation diagrams, the dynamic behaviors are strongly nonperiodic responses at low rotating speeds. As  $l^*$  increases, we can find that the range of nonperiodic motions becomes shorter and amplitude of the systems is also suppressed. Thus, we may conclude that couple-stress fluid can be used to improve dynamics of systems and help the systems escaping nonperiodic responses to be steady.

## Nomenclature

$c$ :	Radial clearance, $c = R - r$
$C$ :	Damping coefficient of the gear mesh
$C_1$ :	Damping coefficients of the supported structure for bearing 1
$C_2$ :	Damping coefficients of the supported structure for bearing 2
$C_{1p}$ :	Dimensionless parameter, $C_{1p} = m_1/m_p$
$C_{01}$ :	Dimensionless parameter, $C_{01} = K/k_1$
$C_{2p}$ :	Dimensionless parameter, $C_{2p} = m_2/m_p$
$C_{02}$ :	Dimensionless parameter, $C_{02} = K/k_2$
$e$ :	Static transmission error and varies as a function of time
$e_i$ :	Offset of the journal center of the rotor relative to the $X$ -coordinate direction
$f$ :	Dimensionless parameter, $f = m_p g / dK$
$f_g$ :	Dimensionless parameter, $f_g = Kg / dm_p$
$f_e, f_\varphi$ :	Components of the fluid film force in radial and tangential directions
$g$ :	Acceleration of gravity
$K$ :	Stiffness coefficient of the gear mesh
$K_{11}, K_{12}$ :	Stiffness coefficients of the springs supporting the two bearing housings for bearing 1
$K_{21}, K_{22}$ :	Stiffness coefficients of the springs supporting the two bearing housings for bearing 2
$K_{p1}, K_{p2}$ :	Stiffness coefficients of the shafts
$L$ :	Bearing length
$m_1$ :	Mass of the bearing housing for bearing 1
$m_2$ :	Mass of the bearing housing for bearing 2
$m_p$ :	Mass of the pinion
$m_g$ :	Mass of the gear
$O_1$ :	Geometric centers of the bearing 1
$O_2$ :	Geometric centers of the bearing 2
$O_{j1}$ :	Geometric centers of the journal 1
$O_{j2}$ :	Geometric centers of the journal 2
$O_g$ :	Center of gravity of the gear
$O_p$ :	Center of gravity of the pinion
$p$ :	Pressure distribution in the fluid film
$R$ :	Inner radius of the bearing housing
$r$ :	Radius of the journal
$s$ :	Rotational speed ratio, $s = (\omega^2/\omega_n^2)^{1/2}$

$s_1$ :	Dimensionless parameter, $s_1^2 = C_{o1}C_{1p}s^2$
$s_2$ :	Dimensionless parameter, $s_2^2 = C_{o2}C_{2p}s^2$
$X, Y, Z$ :	Horizontal, vertical and axial coordinates
$x_j, y_j$ :	$X_j/c, Y_j/c, j = 1, 2, j1, j2, p, g$
$\alpha_1$ :	Dimensionless parameter, $\alpha_1 = K_{12}d^2K/m_1m_p$
$\alpha_2$ :	Dimensionless parameter, $\alpha_2 = K_{22}d^2K/m_2m_p$
$\xi_1$ :	Dimensionless parameter, $\xi_1 = C_1/2\sqrt{K_1m_1}$
$\xi_2$ :	Dimensionless parameter, $\xi_2 = C/2\sqrt{Km_p}$
$\xi_3$ :	Dimensionless parameter, $\xi_3 = C_m/2\sqrt{Km_p}$
$\xi_4$ :	Dimensionless parameter, $\xi_4 : C/2\sqrt{K/m_p m_g}$
$\xi_5$ :	Dimensionless parameter, $\xi_5 = C_m\sqrt{m_p}/2m_g\sqrt{K}$
$\xi_6$ :	Dimensionless parameter, $\xi_6 = C_2/2\sqrt{K_2m_2}$
$\Lambda$ :	Dimensionless parameter, $\Lambda = K_m/K$
$\Lambda_g$ :	Dimensionless parameter, $\Lambda_g = K_m m_p^2/m_g K^2$
$\rho$ :	Mass eccentricity of the rotor
$\phi$ :	Rotational angle, $\phi = \omega t$
$\omega$ :	Rotational speed of the shaft
$\theta$ :	The angular position
$\mu$ :	Oil dynamic viscosity
$\varepsilon$ :	Eccentricity ratio, $\varepsilon = e/c$
$\omega_n$ :	Natural frequency, $\omega_n = \sqrt{K/m_p}$
$\omega_g$ :	Dimensionless parameter, $\omega_g = \omega_n/8$
$\omega_p$ :	Dimensionless parameter, $\omega_p = \omega_n/4$
$\varphi_i$ :	Attitude angle of the rotor relative to the X-coordinate direction.

## References

- [1] D. R. Oliver, "Load enhancement effects due to polymer thickening in a short model journal bearing," *Journal of Non-Newtonian Fluid Mechanics*, vol. 30, no. 2-3, pp. 185–196, 1988.
- [2] H. A. Spikes, "The behaviour of lubricants in contacts: current understanding and future possibilities," *Proceedings of the Institution of Mechanical Engineers, Part J: Journal of Engineering Tribology*, vol. 208, no. 1, pp. 3–15, 1994.
- [3] E. F. El Shehawey and K. S. Mekheimer, "Couple-stresses in peristaltic transport of fluids," *Journal of Physics D*, vol. 27, no. 6, pp. 1163–1170, 1994.
- [4] N. C. Das, "Elastohydrodynamic lubrication theory of line contacts: couple stress fluid model," *Tribology Transactions*, vol. 40, no. 2, pp. 353–359, 1997.
- [5] N. C. Das, "A study of optimum load-bearing capacity for slider bearings lubricated with couple stress fluids in magnetic field," *Tribology International*, vol. 31, no. 7, pp. 393–400, 1998.
- [6] A. A. Elsharkawy and L. H. Guedouar, "Inverse solution for finite journal bearings lubricated with couple stress fluids," *Tribology International*, vol. 34, no. 2, pp. 107–118, 2001.
- [7] C. H. Hsu, J. R. Lin, and H. L. Chiang, "Combined effects of couple stresses and surface roughness on the lubrication of short journal bearings," *Industrial Lubrication and Tribology*, vol. 55, no. 5, pp. 233–243, 2003.
- [8] M. Lahmar, "Elastohydrodynamic analysis of double-layered journal bearings lubricated with couple-stress fluids," *Proceedings of the Institution of Mechanical Engineers, Part J: Journal of Engineering Tribology*, vol. 219, no. 2, pp. 145–171, 2005.
- [9] C. W. Chang-Jian and C. K. Chen, "Non-linear dynamic analysis of bearing-rotor system lubricating with couple stress fluid," *Proceedings of the Institution of Mechanical Engineers, Part C: Journal of Mechanical Engineering Science*, vol. 222, no. 4, pp. 599–616, 2008.

- [10] L. Vedmar and A. Andersson, "A method to determine dynamic loads on spur gear teeth and on bearings," *Journal of Sound and Vibration*, vol. 267, no. 5, pp. 1065–1084, 2003.
- [11] A. Kahraman and R. Singh, "Non-linear dynamics of a spur gear pair," *Journal of Sound and Vibration*, vol. 142, no. 1, pp. 49–75, 1990.
- [12] H. H. Lin, R. L. Huston, and J. J. Coy, "On dynamic loads in parallel shaft transmission—part 1: modeling and analysis," *Journal of Mechanisms, Transmissions, and Automation in Design*, vol. 110, no. 2, pp. 221–225, 1988.
- [13] K. Y. Yoon and S. S. Rao, "Dynamic load analysis of spur gears using a new tooth profile," *Journal of Mechanisms, Transmissions, and Automation in Design*, vol. 118, pp. 1–6, 1988.
- [14] K. Ichimaru and F. Hirano, "Dynamic behavior of heavy-loaded spur gears," *Journal of Engineering for Industry*, vol. 96, no. 2, pp. 373–381, 1974.
- [15] M. Amabili and A. Fregolent, "A method to identify modal parameters and gear errors by vibrations of a spur gear pair," *Journal of Sound and Vibration*, vol. 214, no. 2, pp. 339–357, 1998.
- [16] H. N. Özgüven and D. R. Houser, "Mathematical models used in gear dynamics—a review," *Journal of Sound and Vibration*, vol. 121, no. 3, pp. 383–411, 1988.
- [17] H. N. Özgüven and D. R. Houser, "Dynamic analysis of high speed gears by using loaded static transmission error," *Journal of Sound and Vibration*, vol. 125, no. 1, pp. 71–83, 1988.
- [18] Y. Cai and T. Hayashi, "The linear approximated equation of vibration of a pair of spur gears," *Journal of Mechanical Design*, vol. 116, no. 2, pp. 558–564, 1994.
- [19] K. Umezawa, T. Sato, and J. Ishikawa, "Simulation on rotational vibration of spur gears," *Bulletin of the Japan Society of Mechanical Engineers*, vol. 27, no. 223, pp. 102–109, 1984.
- [20] P. D. McFadden and M. M. Toozhy, "Application of synchronous averaging to vibration monitoring of rolling element bearings," *Mechanical Systems and Signal Processing*, vol. 14, no. 6, pp. 891–906, 2000.
- [21] F. L. Litvin, Q. Lian, and A. L. Kapelevich, "Asymmetric modified spur gear drives: reduction of noise, localization of contact, simulation of meshing and stress analysis," *Computer Methods in Applied Mechanics and Engineering*, vol. 188, no. 1, pp. 363–390, 2000.
- [22] Y. H. Guan, M. Li, T. C. Lim, and W. S. Shepard, "Comparative analysis of actuator concepts for active gear pair vibration control," *Journal of Sound and Vibration*, vol. 269, no. 1-2, pp. 273–294, 2004.
- [23] D. Giagopoulos, C. Salpistis, and S. Natsiavas, "Effect of non-linearities in the identification and fault detection of gear-pair systems," *International Journal of Non-Linear Mechanics*, vol. 41, no. 2, pp. 213–230, 2006.
- [24] S. Theodossiades and S. Natsiavas, "On geared rotordynamic systems with oil journal bearings," *Journal of Sound and Vibration*, vol. 243, no. 4, pp. 721–745, 2001.
- [25] S. Theodossiades and S. Natsiavas, "Periodic and chaotic dynamics of motor-driven gear-pair systems with backlash," *Chaos, Solitons & Fractals*, vol. 12, no. 13, pp. 2427–2440, 2001.
- [26] P. Grassberger and I. Procaccia, "Characterization of strange attractors," *Physical Review Letters*, vol. 50, no. 5, pp. 346–349, 1983.